a segregation coefficient = 1. Also, significant doping levels of Cr^{3+} ions can be achieved in the Al system while maintaining high crystal quality. In this regard, the solution series $LiSr_{1-x}Ba_xAlF_6$ should be examined for crystal quality as a function of the level of Ba substitution and to determine the maximum value of x consistent with formation of the colquiriite structure type since $LiBaAlF_6$ crystallizes in a different structure.[8] The presence of Ba atoms should afford larger twist angles and higher cross sections for Cr^{3+} optical emission.

(8) Babel, D. *Z. Anorg. Allg. Chem.* **1974**, *406*, 23.

Acknowledgment. We thank Dr. Stephen A. Payne of Lawrence Livermore Laboratory for supplying crystals. This work was supported by the US National Science Foundation, DMR-8814432. D.A.K. is grateful to the Alfred P. Sloan Foundation for a fellowship, 1989-1991.

Registry No. $LiCaAlF_6$, 35362-46-0; $LiCaGaF_6$, 35361-72-9; $LiCaCrF_6$, 29467-85-4; $LiSrAl_{0.59}Cr_{0.41}F_6$, 141017-13-2; $LiSrGaF_6$, 35361-73-0; $LiSrCrF_6$, 29661-32-3.

Supplementary Material Available: Listing of anisotropic thermal parameters (Table S-1, 2 pages); listing of calculated and observed structure factors (Table S-2, 14 pages). Ordering information is given on any current masthead page.

Thermodynamic Analysis of the Thermal Nitridation of Aluminum Oxide by Ammonia and Methane

Beng Jit Tan,[†,‡] Youming Xiao,[†] and Steven L. Suib*[,†,‡,§]

Department of Chemistry, U-60, University of Connecticut, Storrs, Connecticut 06269-3060; Institute of Materials Science, University of Connecticut, Storrs, Connecticut 06269; and Department of Chemical Engineering, U-60, University of Connecticut, Storrs, Connecticut 06269

Francis S. Galasso

United Technologies Research Center, East Hartford, Connecticut 06108

Received December 5, 1991. Revised Manuscript Received February 21, 1992

Thermodynamic calculations were performed using the SOLGASMIX-PV computer program to determine the possibility of converting aluminum oxide to aluminum nitride using alumina, ammonia, and methane. Conversion diagrams were constructed for the Al_2O_3–NH_3–CH_4 system over a range of reaction conditions such as temperature, total system pressure, and reagent concentrations. The influence of excess hydrogen, based on thermodynamic considerations alone, was also investigated. Formation of a pure AlN phase was predicted in the range 1800–2000 K and total system pressures of 0.1–1.0 atm. Low pressure and excess hydrogen increase the conversion efficiencies of aluminum and nitrogen, thus favoring the formation of pure AlN.

Introduction

In recent years, there has been increasing interest in non-oxide ceramics such as silicon nitride and silicon carbide which possess high-temperature strength and corrosion resistance. Among these, aluminum nitride is currently of great technological importance because of its unique physical properties such as high thermal conductivity (170–320 W/(m K)), close to that of metals[1-6] and over 10 times that of Al_2O_3, low coefficient of thermal expansion (4–5 μm/(m °C)) comparable to silicon and SiC,[1,7] high electrical resistivity (4×10^{11} Ω cm) and high mechanical strength comparable to alumina ceramics. It is a covalent material with a wurtzite-type crystal structure,[8] which is difficult to sinter. Its elastic,[9] mechanical,[10] and electrical[11] properties and its reactions with metals[12,13] have been described.[14] It has extreme hardness (about 3500 kgf mm^{-2}) and a high melting point (2400 °C). AlN has superior physical properties over those of alumina ceramics. It has a low dielectric constant and loss and good mechanical properties and is nontoxic.[15-17] AlN is a semiconductor with a wide bandgap (E_g = 6.2 eV) with a variety of potential applications including electronic devices for high-temperature operation, surface acoustic wave devices, and short-wavelength optoelectronics.

Aluminum nitride powders can be synthesized using a variety of reactions. One of the more common methods for commerical powders is carbothermal reduction and nitridation.[18-21] This involves intimate mixing of alumina

[†] Department of Chemistry.
[‡] Institute of Materials Science.
[§] Department of Chemical Engineering.
* To whom correspondence should be addressed.

(1) Slack, G. A. *J. Phys. Chem. Solids* **1973**, *34*, 321.
(2) Suryanarayana, D. *J. Electron Packag.* **1989**, *111*, 192.
(3) Komeya, K. *Ceram. Bull.* **1984**, *63*, 1158.
(4) Iwasi, N. *Int. J. Hybrid Microelectron.* **1984**, *7*, 49.
(5) Iwasi, N.; Anzai, K.; Shimozaki, K. *Solid State Technol.* **1986**, *Oct*, 135.
(6) Kurokawa, Y.; Utsumi, K.; Takamizawa, H. *J. Am. Ceram. Soc.* **1988**, *71*, 588.
(7) Li, Z.; Bradt, R. C. *J. Am. Ceram. Soc.* **1986**, *69*, 863.
(8) Amma, E. L.; Jeffrey, G. A. *J. Chem. Phys.* **1961**, *34*, 252.
(9) Gerlich, R. D.; Dole, S. L.; Slack, G. A. *J. Phys. Chem. Solids*, **1986**, *47*, 437.
(10) De With, G.; Hattu, N. *J. Mater. Sci.* **1983**, *18*, 503.
(11) Zulfequar, M.; Kumar, A. *J. Mater. Sci. Lett.* **1986**, *5*, 1230.
(12) Rhee, S. K. *J. Am. Ceram. Soc.* **1970**, *53*, 639.
(13) Trontelj, M.; Kolar, D. *J. Am. Ceram. Soc.* **1978**, *61*, 204.
(14) Billy, M. *J. Mexmain Sprechsaal* **1985**, *118*, 245.
(15) Kurokawa, Y.; Utsumi, K.; Takamizawa, H.; Kamata, T.; Noguchi, S. *IEEE Trans. Compon. Hybrids, Manuf. Technol.* **1985**, *CHMT-8*, 248.
(16) Kurokawa, Y.; Hamaguchi, H.; Shimada, Y.; Utsumi, K.; Takamizawa, H. *NEC Res. Dev.* **1987**, *85*, 15.
(17) Kuramoto, N.; Taniguchi, H.; Aso, I. *IEEE Trans. Compon. Hybrids Manuf. Technol.* **1986**, *CHMT-9*, 386.

0897-4756/92/2804-0648$03.00/0

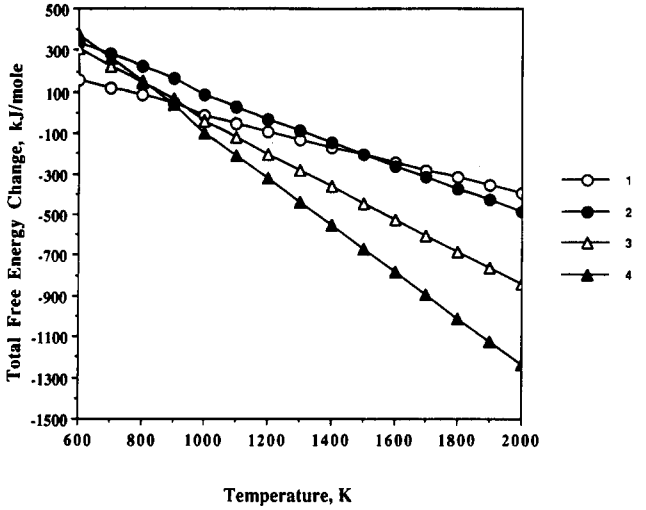

Figure 1. Gibbs free energy change of a few reactions involving the conversion of aluminum oxide to aluminum nitride (see eqs 1–4).

with a source of carbon and heating to above 1100 °C in a nitrogen-containing atmosphere. The most common source of carbon is elemental carbon. Direct nitridation of metallic aluminum with either nitrogen or ammonia to form aluminum nitride powders has also been reported.[22-25] This paper addresses the use of methane as a reducing agent in the nitridation of alumina.

An initial step in determining the process conditions, e.g., reagent concentrations, temperature, and pressure, which would lead to the conversion of Al_2O_3 to AlN is to perform thermodynamic calculations. A conversion diagram can then be constructed for the reaction system so that the positions of the phase boundaries can be accurately determined. The thermodynamic calculations also give the conversion efficiencies for the solid phase, namely, aluminum oxide, as well as the reactant gases, ammonia, and methane.

Thermodynamic Calculations

Several reactions for forming AlN from Al_2O_3 were first considered. A calculation for the temperature range 600–2000 K was then carried out based solely on free energy changes for these reactions:

$$Al_2O_3(s) + 2NH_3(g) \rightarrow 2AlN(s) + 3H_2O(g) \quad (1)$$

$$Al_2O_3(s) + 3C(s) + N_2(g) \rightarrow 2AlN(s) + 3CO(g) \quad (2)$$

$$Al_2O_3(s) + 3C(s) + 2NH_3(g) \rightarrow 2AlN(s) + 3H_2(g) + 3CO(g) \quad (3)$$

$$Al_2O_3(s) + 3CH_4(g) + 2NH_3(g) \rightarrow 2AlN(s) + 3CO(g) + 9H_2(g) \quad (4)$$

The changes in free energy for these systems were solved graphically (Figure 1), and they represent straight line equations. Free energy and temperature are variables, and the coefficients of the gradients of the straight lines are related to entropy. The most feasible reaction of the four considered is reaction 4, in which the net change in free energy obtained is negative at a temperature lower than those of the other three reactions as shown in Figure 1.

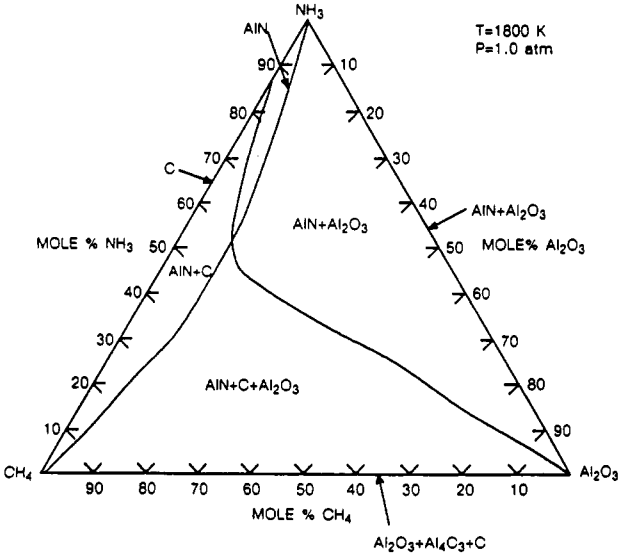

Figure 2. Conversion diagram for the reactant system Al_2O_3 (s)–CH_4 (g)–NH_3 (g) at 1800 K and 1.0 atm showing the region where it is predicted, from only thermodynamic considerations, that pure AlN phase may be formed.

Since reaction 4 is the most feasible reaction for the conversion of alumina to aluminum nitride, the thermodynamic calculations presented in this paper were performed for the Al–N–C–H system. Al_2O_3 and NH_3 were selected as the sources of AlN as they are readily available and inexpensive. CH_4 was selected as the reducing agent. Thus, the overall reaction investigated in this paper is for the Al_2O_3–NH_3–CH_4 system, viz.

$$Al_2O_3(s) + 3CH_4(g) + 2NH_3(g) \rightarrow 2AlN(s) + 3CO(g) + 9H_2(g) \quad (5)$$

Computerized thermodynamic calculations were carried out using the SOLGASMIX-PV program[26] which is a modified version of the SOLGASMIX program.[27] Table I lists the thermodynamic data at 1500, 1800, and 2000 K for the possible gaseous, liquid, and solid species for the Al–N–C–H system. The thermodynamic data for the various species were taken from the JANAF tables.[28] The calculations predict the equilibrium composition of the solid–gas system based on the minimization of the free energy of all the possible gaseous, liquid, and solid species. Numerous chemical equilibrium thermodynamic analyses of this type have already proven useful in understanding chemical processes.[29-32]

The calculations were performed for combinations of Al_2O_3 + NH_3 + CH_4 over the range 0–100 mol % concentrations of the reagents. Reagent compositions were varied by 5 mol % increments. The positions of the phase boundaries were more precisely determined by subsequent calculations using 1 mol % increments. The calculations were again repeated at a pressure of 0.1 atm and with H_2 added for each set of conditions (temperature, pressure,

(18) Lee, B. I.; Einarsrud, M. A. *J. Mater. Sci. Lett.* **1990**, *9*, 1389.
(19) Kuramoto, N.; Taniguchi, H. *J. Mater. Sci. Lett.* **1984**, *3*, 471.
(20) Mitomo, M.; Yoshioka, Y. *Adv. Ceram. Mater.* **1987**, *2*, 253.
(21) Silverman, L. D. *Adv. Ceram. Mater.* **1988**, *3*, 418.
(22) Bensalem, R.; Abid, A.; Sealy, B. J. *Thin Solids Films* **1986**, *143*, 141.
(23) Hotta, N.; Kimura, I.; Tsukuno, A.; Saito, N.; Matsuo, S. *Yogyo Kyokaishi* **1987**, *95*, 136.
(24) Vissokov, G. P.; Brakalov, L. B. *J. Mater. Soc.* **1983**, *18*, 2011.
(25) Kimura, I.; Ichiya, K.; Ishii, M.; Hotta, N.; Kitamura, T. *J. Mater. Sci. Lett.* **1989**, *8*, 303.
(26) Besmann, T. M. *ORNL/TM-5775*; Oak Ridge National Laboratory: Oak Ridge, TN, Apr 1977.
(27) Eriksson, G. *Chem. Scr.* **1975**, *8*, 100.
(28) *JANAF Thermochemical Tables*, 3rd ed., Parts I and II; *J. Phys. Chem. Ref. Data*, Supplement No. 1, **1985**, *14*.
(29) Fischman, G. S.; Petuskey, W. T. *J. Am. Ceram. Soc.* **1985**, *68*, 185.
(30) Kingon, A. I.; Lutz, L. J.; Davis, R. F. *J. Am. Ceram. Soc.* **1983**, *66*, 551.
(31) Besmann, T. M. *J. Am. Ceram. Soc.* **1986**, *69*, 69.
(32) Kingon, A. I.; Lutz, L. J.; Liaw, P.; Davis, R. F. *J. Am. Ceram. Soc.* **1983**, *66*, 558.

Table I. Enthalpy and Entropy Data at 1500, 1800, and 2000 K Used in the SOLGASMIX-PV Calculations

	1500 K		1800 K		2000 K	
species	$\Delta H_f°$, kJ/mol	$S_f°$, J/(mol K)	$\Delta H_f°$, kJ/mol	$S_f°$, J/(mol K)	$\Delta H_f°$, kJ/mol	$S_f°$, J/(mol K)
Al(g)	308.139	-198.419	304.856	-202.212	302.665	-204.404
Al_2(g)	443.573	-300.645	436.634	-308.008	432.003	-312.259
AlOH(g)	-208.836	-287.000	-212.123	-297.153	-214.215	-303.158
AlN(g)	500.905	-286.361	497.471	-293.275	495.166	-297.291
AlO(g)	43.893	-275.465	41.605	-283.221	40.405	-287.909
AlO_2(g)	-102.760	-344.642	-104.875	-355.858	-106.365	-362.370
Al_2O(g)	-187.505	-346.357	-193.581	-357.608	-197.658	-364.126
Al_2O_2(g)	-433.154	-406.430	-438.549	-421.459	-442.229	-430.162
H_2N(g)	184.182	-527.675	183.925	-266.728	183.891	-272.168
H_3N(g)	-55.954	-271.442	-55.439	-283.962	-54.833	-291.525
N_3(g)	421.156	-309.238	423.252	-320.148	424.602	-326.515
CO(g)	-115.229	-248.426	-117.384	-245.912	-118.896	-258.714
C_1(g)	718.415	-191.710	717.373	-195.509	716.577	-197.713
C_2(g)	835.528	-259.869	832.266	-266.750	830.000	-270.801
C_3(g)	802.255	-304.372	795.226	-313.394	790.421	-318.731
C_4(g)	964.753	-338.748	960.404	-353.832	957.248	-362.660
CH(g)	591.314	-233.318	590.329	-240.149	589.723	-244.238
CH_2(g)	379.299	-260.740	377.835	-270.280	376.844	-275.953
CH_3(g)	134.662	-277.327	133.554	-290.082	132.917	-297.727
CH_4(g)	-92.553	-279.763	-92.797	-296.039	-92.709	-305.853
C_2H(g)	470.837	-383.188	468.346	-292.535	466.681	-298.689
C_2H_2(g)	185.216	-298.567	174.353	-312.829	166.980	-321.335
C_2H_4(g)	35.456	-341.877	35.005	-362.460	34.894	-374.791
C_3O_2(g)	-92.921	-417.455	-94.192	-436.706	-95.209	-447.989
C_2O(g)	285.650	-317.732	284.143	-329.043	283.063	-335.695
CO_2(g)	-395.668	-292.199	-396.311	-302.968	-396.784	-309.293
H(g)	224.836	-148.229	226.132	-152.088	226.898	-154.278
H_2(g)	0.000	-178.846	0.000	-171.790	0.000	-188.418
C_5(g)	973.524	-381.756	968.885	-401.096	965.493	-412.421
N(g)	478.462	-186.882	497.411	-190.672	479.990	-192.863
N_2(g)	0.000	-241.880	0.000	-248.304	0.000	-252.074
NO(g)	90.518	-262.703	90.522	-269.282	90.494	-273.128
NO_2(g)	32.603	-315.715	32.940	-325.861	33.111	-331.788
NO_3(g)	77.155	-361.631	79.411	-376.308	80.809	-384.856
N_2O(g)	85.902	-299.825	87.488	-310.577	88.527	-216.871
N_2O_3(g)	90.173	-444.794	92.854	-462.941	94.557	-473.537
N_2O_4(g)	24.097	-474.997	29.550	-498.193	33.110	-511.743
N_2O_5(g)	32.741	-553.434	38.487	-580.176	42.064	-595.711
NH(g)	376.420	-230.275	376.488	-236.528	376.551	-240.233
N_2H_2(g)	207.275	-303.767	208.504	-316.936	209.457	-324.781
N_2H_4(g)	91.270	-369.884	94.871	-390.490	97.538	-402.810
O(g)	254.171	-195.254	254.884	-199.053	255.299	-201.247
O_2(g)	0.000	-258.068	0.000	-264.796	0.000	-268.748
O_3(g)	144.750	-319.469	145.419	-330.349	145.784	-336.469
N_2C_4(g)	539.082	-565.514	538.075	-489.052	537.186	-502.844
NC(g)	259.742	-253.732	251.791	-260.333	246.516	-264.251
CNO(g)	160.418	-313.861	160.165	-324.715	159.895	-331.057
CN_2(g)	585.822	-312.746	585.113	-323.351	584.786	-329.573
H_2O(g)	-250.265	-250.620	-251.138	-259.451	-251.575	-264.769
AlC(g)	663.291	-281.128	657.830	-288.030	654.110	-292.038
AlN(s)	-328.856	-90.137	-328.425	-99.399	-328.119	-104.290
Al_2O_3(l)	-1623.274	-255.138	-1601.197	-290.228	-1586.658	-310.507
Al_2O_3(s)	-1662.040	-242.229	-1655.675	-267.762	-1651.174	-282.751
Al(l)	0.000	-86.273	0.000	-92.062	0.000	-95.408
Al_4C_3(s)	-270.825	-346.577	-274.774	-380.621	-277.278	-400.550
C(s)	0.000	-33.718	0.000	-38.149	0.000	-40.771

and reagent concentrations) previously evaluated. Four sets of calculations were performed, each for 1500 and 2000 K, namely:

(a) at total gas pressure of 1.0 atm

(b) at total gas pressure of 0.1 atm

(c) at total gas pressure of 1.0 atm with excess hydrogen added

(d) at total gas pressure of 0.1 atm with excess hydrogen added

Results and Discussion

(A) Conversion/Phase Diagrams. Conversion diagrams, such as the one shown in Figure 2, can be constructed from the results of the thermodynamic calculations. These diagrams show the equilibrium solid phase(s) as a function of reagent concentrations for a specific temperature and total gas pressure for the reagent system NH_3–Al_2O_3–CH_4. Conversion diagrams at 1500 K predicted that pure AlN could not be formed at the conditions investigated. Thus emphasis was placed on higher temperature calculations. The conversion diagram in Figure 2 is for a temperature of 1800 K and 1 atm total gas pressure. Thermodynamic calculations predict that the conversion diagram consists of four regions. On the left-hand side is a two-phase region marked AlN + C. In this region complete conversion of Al_2O_3 to AlN occurs with co-deposition of C from the thermal decomposition/oxidation of methane. On the right-hand side is a two-phase region, marked AlN + Al_2O_3, in which incomplete conversion of the Al_2O_3 to AlN takes place.

Sandwiched between these two regions is the area of interest. Within this area, conversion of Al_2O_3 to AlN

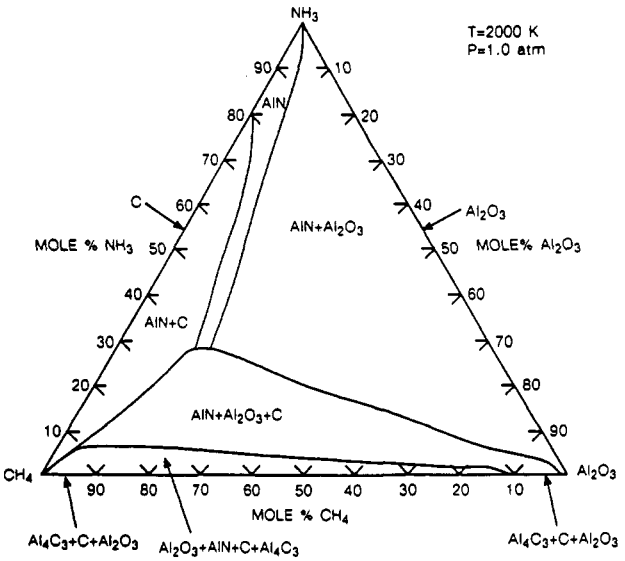

Figure 3. Conversion diagram obtained at higher temperature (2000 K, 1.0 atm) increases the area of the pure AlN phase region.

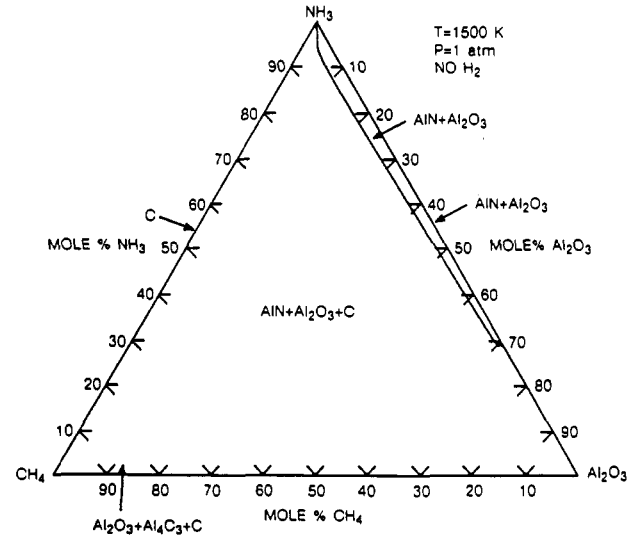

Figure 4. No pure AlN phase region is predicted from only thermodynamic considerations alone at 1500 K and 1.0 atm.

proceeds to completion and pure AlN is formed. Reagent composition for this one-phase region includes 0–10 mol % Al_2O_3, 50–100 mol % NH_3, and 0–40 mol % CH_4. The fourth region is a three-phase region marked AlN + C + Al_2O_3 found at the bottom half of the phase diagram.

At the corners of the triangle at 100 mol % NH_3 and 100 mol % CH_4, no solid phase is present and only gases (NH_3 and CH_4, respectively) are present at equilibrium. At 100 mol % Al_2O_3, the only solid phase present is Al_2O_3. No gases are present at equilibrium. For the line joining the two corners of 100 mol % NH_3 and 100 mol % CH_4, the only solid phase present is C. Two solid phases are predicted, namely, AlN and Al_2O_3, along the line joining 100 mol % Al_2O_3 and 100 mol % NH_3, while it is predicted that three phases (C + Al_2O_3 + Al_4C_3) exist at equilibrium along the line joining 100 mol % CH_4 and 100 mol % Al_2O_3.

To determine the effect of reaction conditions such as temperature, total system pressure, and hydrogen concentration on the conversion of Al_2O_3 to AlN, numerous additional conversion diagrams were constructed. Several of those diagrams are presented in this paper to illustrate the effects of changes in the conversion process.

The influence of higher temperature (2000 K) at 1.0 atm results in an increase in area of the AlN region over that at 1800 K as shown in Figure 3. The length of the pure AlN region is increased. Thus the minimum concentration of ammonia required in the reagent composition for complete conversion of Al_2O_3 to AlN is reduced as the temperature increases from 1800 to 2000 K. There is also a large increase in the area of the AlN + Al_2O_3 region accompanied by a large decrease in area of the AlN + Al_2O_3 + C region. A four-phase AlN + C + Al_2O_3 + Al_4C_3 region is also predicted at the bottom of the triangle. However, Al_2O_3 is the only solid phase predicted along the line joining 100 mol % Al_2O_3 and 100 mol % NH_3. No AlN is predicted to form along this line at 2000 K.

The conversion diagram for the reaction temperature of 1500 K is shown in Figure 4. No pure AlN region is predicted at 1500 K and 1.0 atm total system pressure.

A decrease in pressure while maintaining the temperature at 1800 K results in an increase in area of the AlN conversion region (Figure 5). Reagent composition for the complete conversion of Al_2O_3 into pure AlN now includes 0–19 mol % Al_2O_3, 45–96 mol % NH_3, and 5–55 mol % CH_4. There is also an increase in the areas of the two-phase regions of AlN + C and AlN + Al_2O_3 accompanied

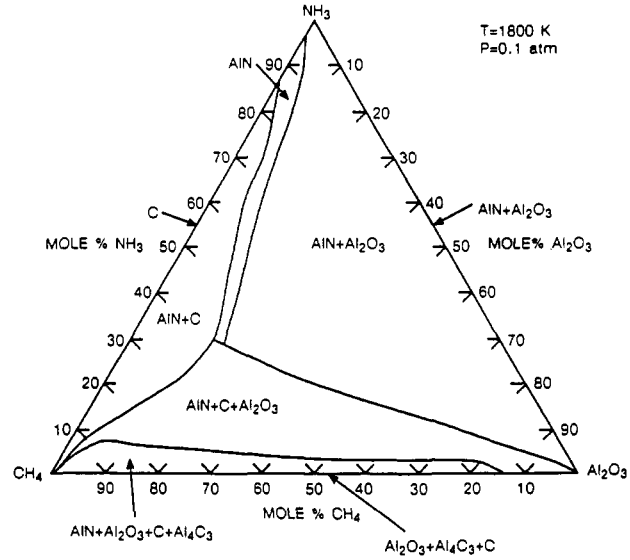

Figure 5. Decreasing the total system pressure to 0.1 atm while maintaining the temperature at 1800 K results in an increase in the area of the pure AlN phase region and the appearance of a four-phase region (AlN, C, Al_2O_3, and Al_4C_3) at the bottom of the diagram.

by a decrease in the area of the three-phase (AlN + C + Al_2O_3) region. The boundary between the two-phase and three-phase regions is pushed down toward the base of the triangle.

Low total system pressure also results in the introduction of a four-phase region marked AlN + C + Al_2O_3 + Al_4C_3 at the bottom of the triangle. Thus at low NH_3 concentrations, the reduced alumina combines with carbon to form Al_4C_3. The latter is stable at low pressure. The solid phases predicted along the lines joining the three corners of the triangle remain the same, namely, C along the line joining 100 mol % NH_3 and 100 mol % CH_4, AlN, and Al_2O_3 along the line joining 100 mol % Al_2O_3 and 100 mol % NH_3 and C + Al_2O_3 + Al_4C_3 along the line joining 100 mol % CH_4 and 100 mol % Al_2O_3.

The effect resulting from the reduction in the system pressure becomes more pronounced at higher temperature. Thermodynamic calculations predict that increasing the temperature to 2000 K at low pressure further increases the area for complete conversion to AlN (Figure 6). This area is larger than those at 1800 K under 1.0 atm as well

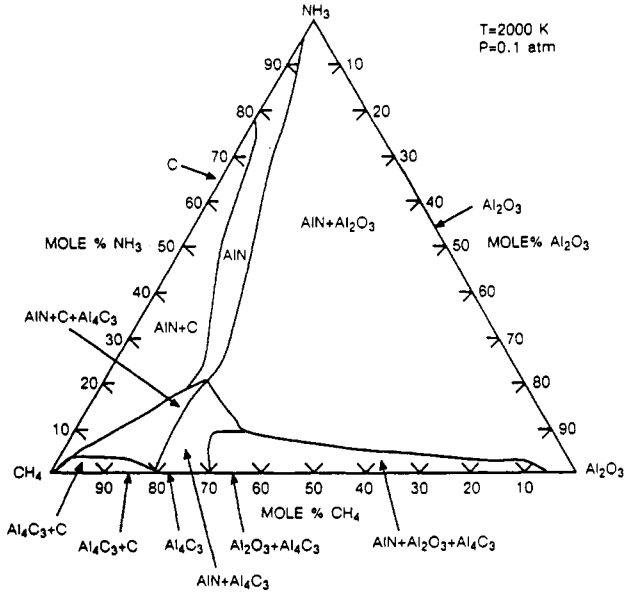

Figure 6. Effect of reduced system pressure (0.1 atm) becomes even more pronounced at higher temperature (2000 K). The area of the pure AlN region increases further. The three-phase (AlN, C, Al_2O_3) region is absent and various other two- and three-phase regions (AlN, C, Al_2O_3 and Al_4C_3) begin to develop.

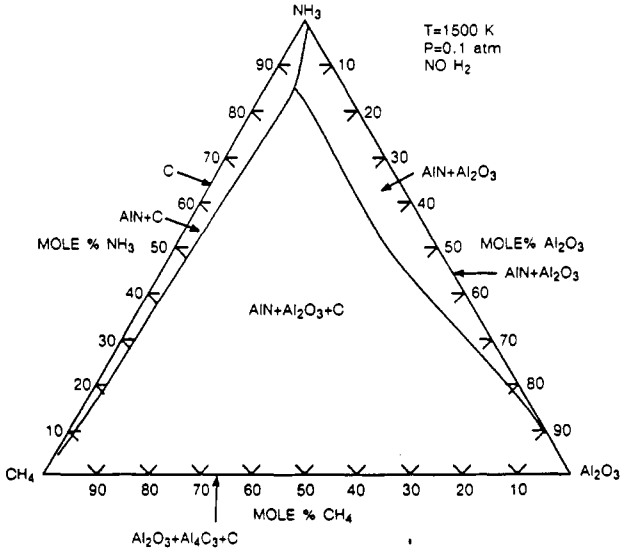

Figure 7. Low-temperature (1500 K) and low-pressure (0.1 atm) do not favor the formation of pure AlN phase. The major portion of the triangle consists of the three-phase AlN–C–Al_2O_3 region.

as 0.1 atm. The area of the AlN + Al_2O_3 region is also substantially increased. In addition the AlN + Al_2O_3 + C region is absent. Instead various two- and three-phase regions consisting of various combinations of AlN, C, Al_2O_3, and Al_4C_3 phases (but not AlN + Al_2O_3 + C) are predicted. In contrast to the conversion diagram at 1800 K and 0.1 atm, no four-phase region (such as AlN + C + Al_2O_3 + Al_4C_3) is predicted.

The only solid phase predicted along the line joining 100 mol % NH_3 and 100 mol % CH_4 is still C. Note that Al_2O_3 is the only solid phase predicted along the line joining 100 mol % Al_2O_3 and 100 mol % NH_3. No AlN phase is predicted along this entire line. Different phases are predicted along the line joining 100 mol % CH_4 and 100 mol % Al_2O_3.

At a reaction temperature of 1500 K, no pure AlN is formed at a total system pressure of 0.1 atm. The major portion of the conversion diagram consists of the AlN–C–Al_2O_3 region (Figure 7).

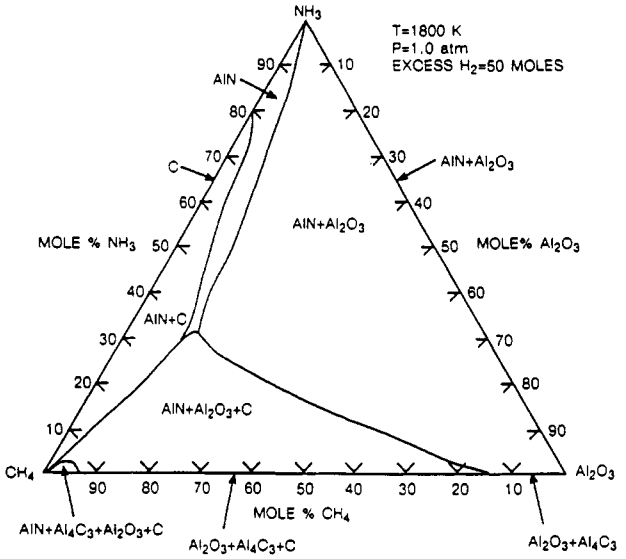

Figure 8. Thermodynamic calculations predict that introduction of excess hydrogen (50 mol) at 1800 K and 1.0 atm total system pressure results in an increase in the area of the pure AlN region.

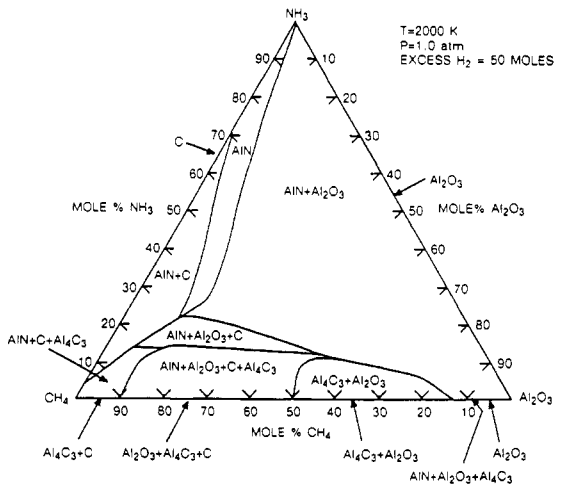

Figure 9. Effect of introduction of excess hydrogen (50 mol) on the formation of pure AlN phase is even more prominent at higher temperature (2000 K, 1 atm pressure). The area of the pure AlN phase region is increased and various two-, three-, and four-phase regions are formed.

Figure 8 is the conversion diagram obtained when hydrogen is added to the system at 1800 K and 1 atm. The area of the one-phase AlN region increases, accompanied by a decrease in the areas of the AlN + C and AlN + C + Al_2O_3 regions. In fact, no deposition of C occurs in the AlN + Al_2O_3 region until a minimum of 15 mol % of CH_4 is reached. A small four-phase region marked C + Al_2O_3 + Al_4C_3 + AlN is predicted at high mol % of CH_4 (>95 mol %) and low Al_2O_3 and NH_3 concentrations (left-hand corner of the triangle). An increase in the area of the AlN + Al_2O_3 region is also noted. Other changes observed include the introduction of several phase regions along the line joining 100 mol % CH_4 and 100 mol % Al_2O_3.

Again, C is still the only solid phase predicted along the line joining 100 mol % NH_3 and 100 mol % CH_4, AlN and Al_2O_3 are predicted along the line joining 100 mol % Al_2O_3 while different phases are predicted along the line joining 100 mol % CH_4 and 100 mol % Al_2O_3.

Increasing the reaction temperature to 2000 K in the presence of excess hydrogen at 1.0 atm results in a further increase in areas of the AlN and AlN + Al_2O_3 regions over those at 1800 K. This is shown in Figure 9. The area of

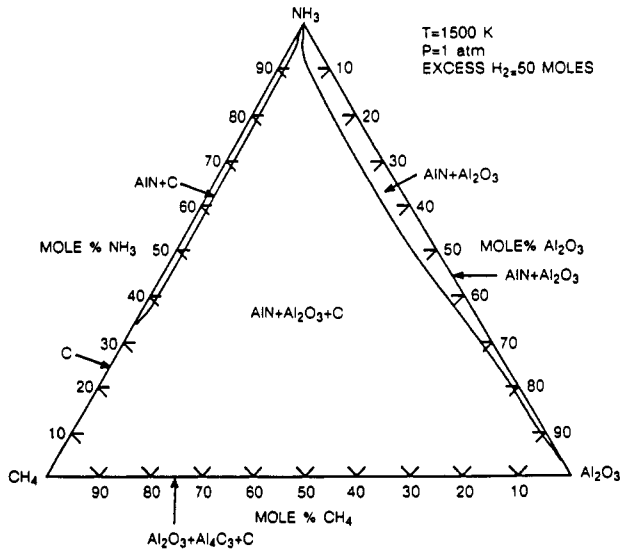

Figure 10. At low temperature (1500 K, 1 atm), the introduction of excess hydrogen (50 mol) has no effect in favoring the formation of a pure AlN phase region. No pure AlN phase region is predicted from only thermodynamic considerations.

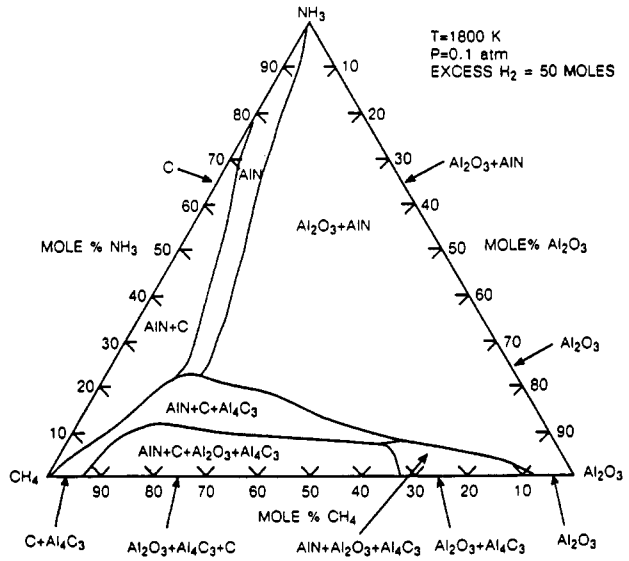

Figure 11. Addition of hydrogen (50 mol) at low pressure (0.1 atm total system pressure) and 1800 K increases the area of the AlN region while the areas of the other regions decrease.

the AlN + Al_2O_3 + C region is substantially decreased. The conversion diagram becomes more complicated with the introduction of various different two-, three-, and four-phase regions consisting of combinations of AlN, C, Al_2O_3, and Al_4C_3 phases. The areas of the AlN, AlN + C, and AlN + Al_2O_3 regions are very similar to those of the conversion diagram for 1800 K and at 0.1 atm with excess hydrogen present.

The only solid phase predicted along the line joining 100 mol % NH_3 and 100 mol % CH_4 is again C. Al_2O_3 is the only solid phase predicted along the line joining 100 mol % Al_2O_3 and 100 mol % NH_3 while different phases are predicted along the line joining 100 mol % CH_4 and 100 mol % Al_2O_3.

However, at a temperature of 1500 K, the introduction of excess hydrogen (50 mol) at a total system pressure of 1.0 atm does not favor the formation of pure AlN (Figure 10).

The conversion diagram obtained for a decrease in the total pressure of the system to 0.1 atm in the presence of excess hydrogen at 1800 K is shown in Figure 11. Again

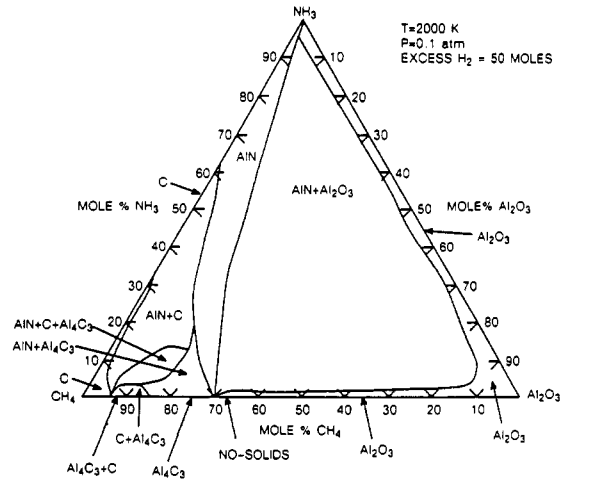

Figure 12. Addition of hydrogen (50 mol) at high temperature (2000 K) and a low system pressure of 0.1 atm further results in an increase in the area of the AlN region.

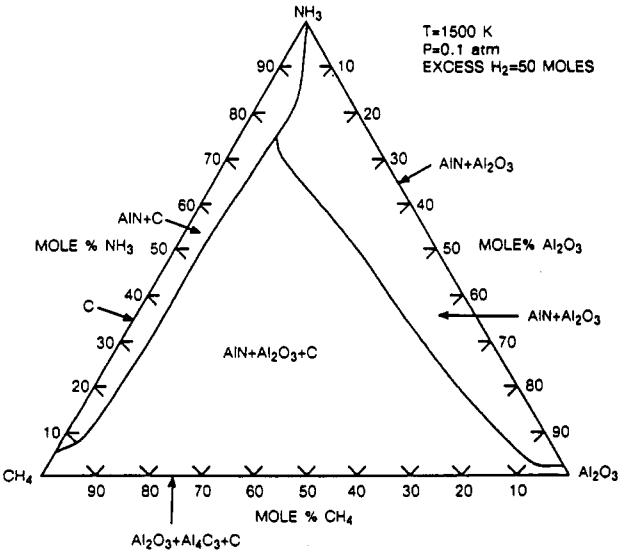

Figure 13. Addition of hydrogen (50 mol) and low system pressure (0.1 atm) have no effect in favoring the formation of a pure AlN phase region at low temperature (1500 K). No pure AlN phase region is predicted by thermodynamic considerations alone.

there is an increase in the area of the pure AlN phase region. In fact, for all the cases considered so far, thermodynamic calculations predict that low pressure together with an excess of hydrogen results in the largest area of the region for complete conversion of Al_2O_3 to AlN at 1800 K. The other regions, namely, AlN + C, AlN + Al_2O_3, and AlN + C + Al_2O_3 regions, decrease in area. In addition, two more regions are predicted, a four-phase AlN + C + Al_2O_3 + Al_4C_3 region and a three-phase AlN + Al_2O_3 + Al_4C_3 region is found at the bottom of the triangle.

At 1800 K, at 0.1 atm, and in the presence of excess hydrogen, C is still the only solid phase predicted along the line joining 100 mol % NH_3 and 100 mol % CH_4 while different phases are predicted along the line joining 100 mol % CH_4 and 100 mol % Al_2O_3. AlN and Al_2O_3 phases are predicted along the line joining 100 mol % Al_2O_3 and 100 mol % NH_3 up to 64 mol % Al_2O_3. At higher mol % Al_2O_3 the only solid phase predicted along this line is Al_2O_3.

The conversion diagram of Figure 12 shows that a combination of high temperature (2000 K), low system pressure (0.1 atm), and excess hydrogen (50 mol) results in a significant increase in the area of the pure AlN region. In contrast, at a low reaction temperature (1500 K) while

Table II. Conversion/Deposition Efficiencies for Aluminum, Nitrogen, and Carbon as a Function of Methane to Aluminum Oxide and Ammonia to Aluminum Oxide Molar Ratios

CH_4:Al_2O_3 molar ratio	Al conv eff		N conv eff		C dep eff	
	NH_3:Al_2O_3 = 8	NH_3:Al_2O_3 = 2	NH_3:Al_2O_3 = 8	NH_3:Al_2O_3 = 2	NH_3:Al_2O_3 = 8	NH_3:Al_2O_3 = 2
1	0.33	0.25	0.07	0.20	0.00	0.00
3	1.00	0.81	0.20	0.67	0.00	0.00
9	1.00	1.00	0.20	0.80	0.67	0.54

maintaining the other reaction conditions (low pressure and excess hydrogen), no pure AlN is formed (Figure 13).

(B) Conversion Efficiencies. In this work, conversion efficiency is defined as the fraction of reagent that is converted to AlN. For example, if 0.2 mol of AlN is formed for every 1.0 mol of NH_3 introduced into the reaction system, the conversion efficiency of NH_3 into AlN is 0.2. Similarly, we define deposition efficiency for CH_4 as the fraction of CH_4 that is deposited as solid graphite. A knowledge of C deposition efficiency will help in determining the experimental conditions that will not facilitate the deposition of C and hence eliminate the need to burn off the C deposited during the conversion process. Thermodynamic data at 1500 K were used in all calculations involving conversion/deposition efficiencies over the temperature range of interest (1000–2000 K).

Parts A and B of Figure 14 summarize the conversion efficiency for Al and N, respectively, over the temperature range 1000–2000 K. The NH_3/Al_2O_3 molar ratio is fixed at 4, and the plots were determined as a function of temperature and CH_4/Al_2O_3 molar ratios. The shape of the plots for Al and N conversion efficiencies are identical but they differ in the conversion efficiency values for a particular temperature and CH_4/Al_2O_3 molar ratio. Table II compares the Al and N conversion efficiencies for NH_3/Al_2O_3 molar ratios of 8 and 2 with respect to CH_4/Al_2O_3 molar ratios.

It can be seen from Table II and Figure 14A,B that an increase in CH_4/Al_2O_3 molar ratio causes an initial increase in the Al and N conversion efficiencies up to a CH_4/Al_2O_3 molar ratio of 3. Higher CH_4/Al_2O_3 molar ratios (>3) do not increase the Al and N conversion ratios much further even with increasing NH_3/Al_2O_3 ratios. For a fixed NH_3/Al_2O_3 ratio, a change in CH_4/Al_2O_3 molar ratio does not significantly alter the Al and N conversion efficiencies at low reaction temperatures, but as the reaction temperature increases above 1700 K, an increase in CH_4/Al_2O_3 molar ratio increases the Al and N conversion efficiencies considerably.

Figure 14C summarizes the thermodynamic predictions for the C deposition efficiency for the same reactant molar ratios as those of Figure 14A,B and over the temperature range 1000–2000 K. The C deposition efficiency increases initially to a maximum at about 1200 K for all CH_4/Al_2O_3 molar ratios. It then levels off at a deposition efficiency of around 0.9–0.95 until a temperature of 1500 K is reached. Above 1500 K the deposition efficiency decreases to a certain minimum value at 1800 K and levels off even at higher temperatures. This minimum value can be as low as 0 for CH_4/Al_2O_3 molar ratio ≤2.69 but increases with increasing CH_4/Al_2O_3 molar ratio such that, at a CH_4/Al_2O_3 molar ratio of 15.0, the C deposition efficiency levels off to a minimum value of 0.78. Thus, judging from the results of Figure 14, it is advantageous to employ low CH_4/Al_2O_3 molar ratios and a reaction temperature ≥1800 K as less C deposition occurs with maximum Al and N conversion efficiencies.

Table III summarizes the NH_3/Al_2O_3 molar ratios and the corresponding CH_4/Al_2O_3 molar ratio in order to achieve on Al conversion efficiency of 1.0 at 1800 K. Maximum Al and N conversion efficiencies occur at lower

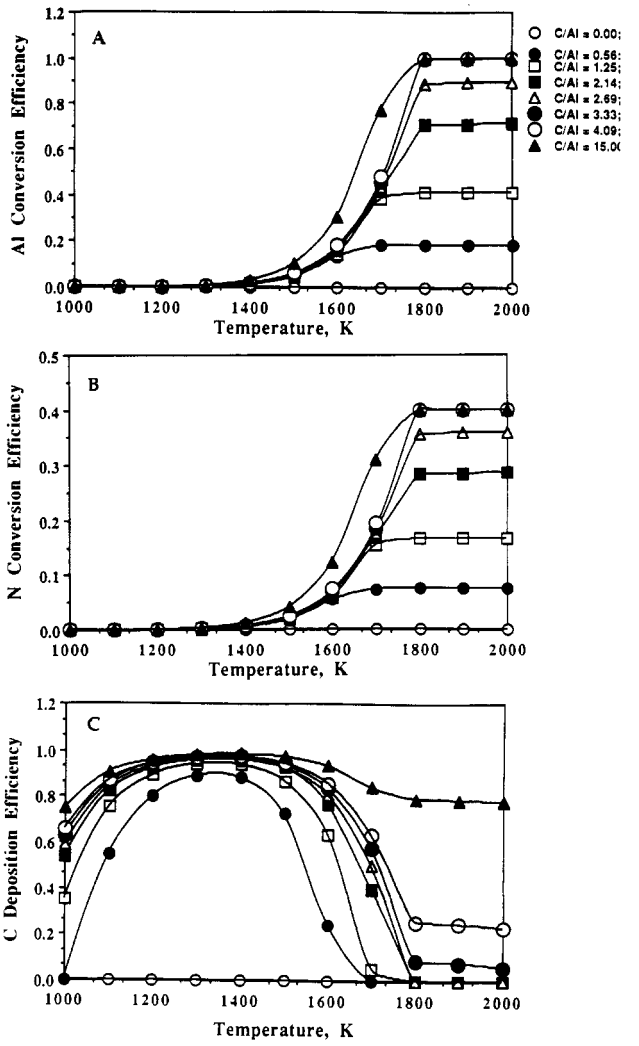

Figure 14. (A) Aluminum conversion efficiency as a function of temperature. The Al conversion efficiency increases with temperature until a maximum is reached around 1850 K. Each curve represents the conversion efficiency response of a specific CH_4/Al_2O_3 ratio. (B) Nitrogen conversion efficiency as a function of temperature. The N conversion efficiency also increases with temperature until a maximum is reached around 1850 K. (C) Carbon deposition efficiency as a function of temperature. The C deposition efficiency is high at low temperatures and falls off at higher temperature range (>1500 K). Increasing the CH_4/Al_2O_3 ratio favors the deposition efficiency.

Table III. Methane to Aluminum Oxide Ratio for Aluminum Conversion Efficiency of Ammonia to Aluminum Oxide Molar Ratio

NH_3:Al_2O_3 molar ratio	CH_4:Al_2O_3 molar ratio for Al conv Eff of 1.0	NH_3:Al_2O_3 molar ratio	CH_4:Al_2O_3 molar ratio for Al conv Eff of 1.0
2	.90	6	3.8
4	4.1	8	3.0

CH_4/Al_2O_3 molar ratio with increase in NH_3/Al_2O_3 molar ratios. Higher temperatures are required to attain maximum Al and N conversion efficiencies at low NH_3/Al_2O_3 molar ratios.

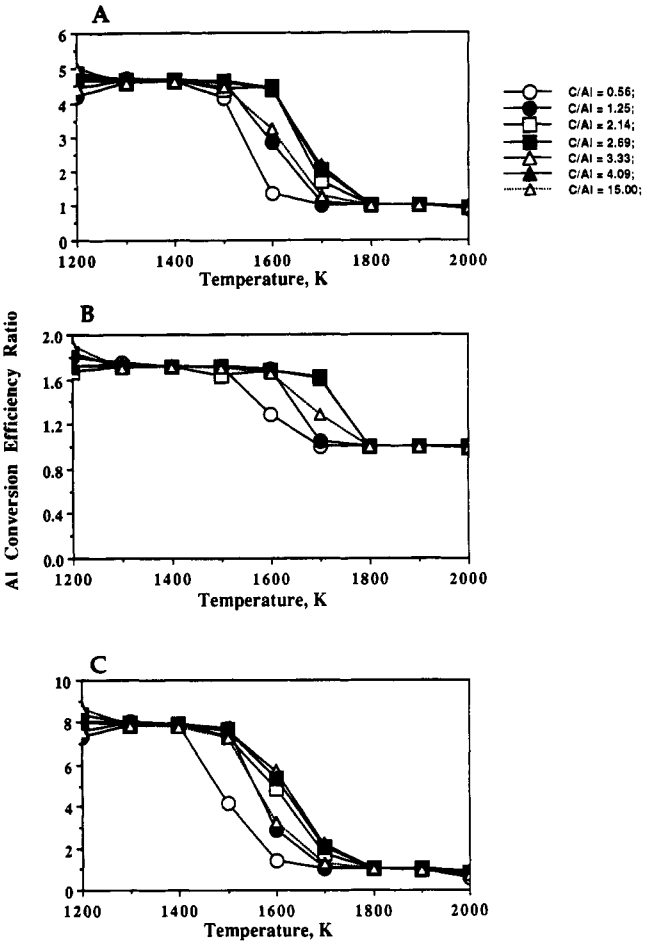

Figure 15. Effects of low pressure (0.1 atm) (A), addition of excess hydrogen (50 mol) (B), and a combination of low pressure (0.1 atm) and excess hydrogen (50 mol) (C) on the Al conversion efficiency ratio. Each curve represents the conversion efficiency ratio response for a specific CH_4/Al_2O_3 ratio as indicated in the figure. Note the differences in the y-axis scale for each figure.

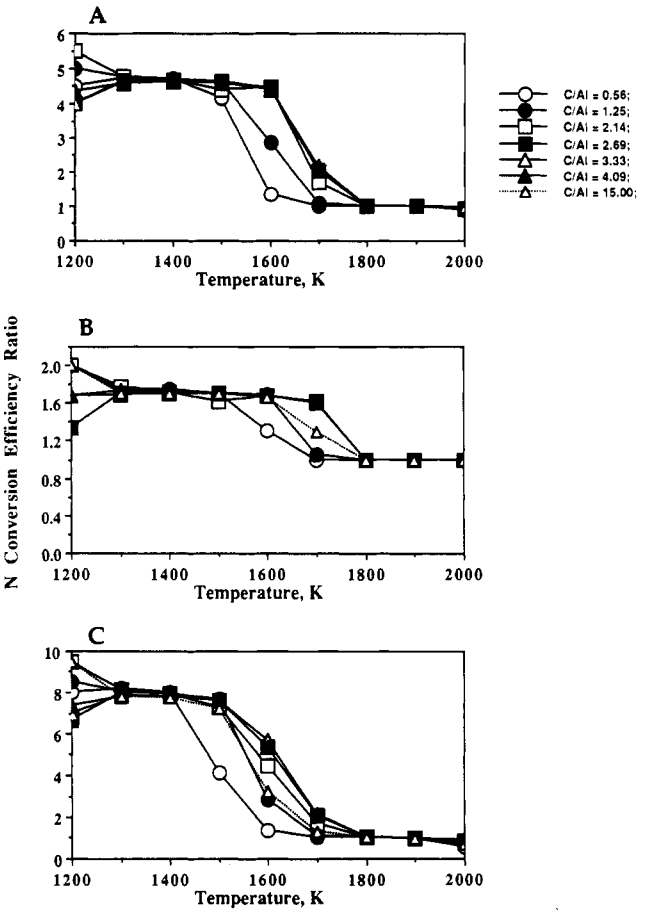

Figure 16. Effects of low pressure (0.1 atm) (A), addition of excess hydrogen (50 mol) (B), and a combination of low pressure (0.1 atm) and excess hydrogen (50 mol) (C) on the N conversion efficiency ratio. Each curve represents the conversion efficiency ratio response for a specific CH_4/Al_2O_3 ratio as indicated in the figure. Note the differences in the y-axis scale for each figure.

(1) Effect of Low Pressure and Excess Hydrogen on Al and N Conversion Efficiencies. Figures 15 and 16 compare the effects of low pressure and addition of hydrogen on the Al and N conversion efficiency ratios, respectively. The conversion/deposition efficiency ratio for a specific temperature is defined as the ratio of the conversion efficiency for a particular set of conditions (pressure and/or introduction of excess hydrogen) to the conversion/deposition efficiency obtained at 1.0 atm pressure at that temperature with no excess hydrogen introduced into the system.

A general trend observed in both Figures 15 and 16 is that the Al and N conversion efficiency ratios are higher than 1.0 for temperatures lower than 1700 K for all CH_4/Al_2O_3 molar ratios. In other words, there is better conversion of NH_3 and Al_2O_3 into AlN at lower pressure and/or with the introduction of excess hydrogen for the temperature range between 1200 and 1700 K. Above 1700 K the ratio is about 1.0. Thus at high temperatures (>1700 K), decreasing the pressure and/or introducing excess hydrogen into the system does not increase the conversion efficiencies. Comparison of Figures 15 and 16 reveals that the trends in the Al conversion efficiency ratio are identical to those of the N conversion efficiency ratio, with only a slight difference in the value of the ratio at 1200 K.

A closer examination of Figures 15 and 16 reveals the following. For all CH_4/Al_2O_3 ratios, decreasing the total pressure of the system to 0.1 atm affects the Al and N conversion efficiencies in the following manner (Figures 15A and 16A):

(a) Between 1200 and 1500 K, the Al and N conversion efficiency ratios at P_{tot} = 0.1 atm were 4–6 times that at P_{tot} = 1.0 atm.

(b) Between 1500 and 1700 K, Al and N conversion efficiency ratios decrease rapidly.

(c) At temperatures ≥1800 K, the ratio is approximately 1.0 (0.9–1.0).

Addition of excess hydrogen (50 mol) into the Al_2O_3 + CH_4 + NH_3 system (Figures 15B and 16B) leads to Al and N conversion efficiency ratios >1.0 for reaction temperatures between 1200 and 1700 K for all CH_4/Al_2O_3 ratios. However, the maxima in Al and N conversion efficiency ratios for the case in which excess hydrogen is present are not as large as that when the P_{tot} was decreased to 0.1 atm. (The Al and N conversion efficiency ratio maxima are no more than a factor of 2.0. In most cases the ratio increased only up to 1.7 as compared to 4–6 in the case of decreasing the total pressure to 0.1 atm.). In other words, a decrease in P_{tot} is more effective in enhancing the conversion of Al_2O_3 to AlN than the introduction of hydrogen into the system. The ratios decrease rapidly at temperatures above 1500 K to a value of 1 (±0.5) at 1800 K. There is no enhanced Al or N conversion efficiency above a reaction temperature of 1800 K, i.e., the ratio of the Al and N conversion efficiencies with and without the addition of hydrogen remained at 1.0 for all CH_4/Al_2O_3 ratios.

Thermodynamic calculations predict that for a total system pressure of 0.1 atm in the presence of excess hydrogen (Figures 15C and 16C), the maxima of the Al and N conversion efficiency ratios are even much higher than

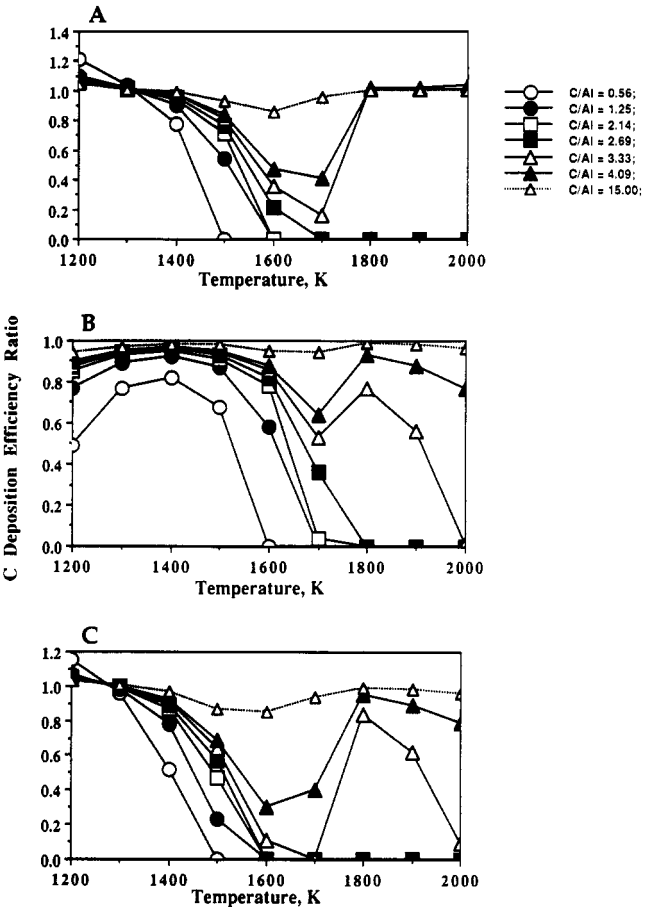

Figure 17. Effects of low pressure (0.1 atm) (A), addition of excess hydrogen (50 mol) (B), and a combination of low pressure (0.1 atm) and excess hydrogen (50 mol) (C) on the C deposition efficiency ratio. Each curve represents the conversion efficiency ratio response for a specific CH_4/Al_2O_3 ratio as indicated in the figure.

those obtained at low pressure alone (around 8 as compared to around 4.5 in the case of low pressure alone). However, the ratios decrease rapidly to approximately 1.0 (±0.5) above 1500 K.

(2) *Effect of Low Pressure and Excess Hydrogen on C Deposition Efficiencies.* Figure 17 shows the plots for the C deposition efficiency ratios at low pressure (P_{tot} = 0.1 atm) and/or in the presence of excess hydrogen. At low pressure (P_{tot} = 0.1 atm, Figure 16A), the C deposition efficiency ratio is greater than 1.0 at 1200 K but decreases rapidly to a minimum value at 1700 K. This minimum C deposition efficiency ratio value at 1700 K increases with increasing CH_4/Al_2O_3 molar ratios. This increase in the minimum C efficiency value with increase in CH_4/Al_2O_3 molar ratios is expected as an excess of CH_4 beyond the CH_4 concentration required to serve as the reducing agent would lead to decomposition of CH_4 to C at high temperature. The temperature at which the minimum C deposition efficiency ratio is attained decreases with increasing CH_4/Al_2O_3 molar ratios such that at a CH_4/Al_2O_3 molar ratio of 15.00, the minimum value is obtained at 1600 K. For low CH_4/Al_2O_3 molar ratio (≤2.69), low pressure prevents C deposition and the ratio falls to 0 at 1800 K and continues to do so even at higher temperatures. For CH_4/Al_2O_3 molar ratios ≥ 2.69, the C deposition ratio increases back to a value of 1.0.

A closer look at the C deposition efficiency ratio for a system pressure of 0.1 atm reveals the following:

(a) For low CH_4/Al_2O_3 ratios (0.47–3.00), deposition ratios decrease with increasing reaction temperatures. For these CH_4/Al_2O_3 molar ratios, the deposition ratio is <1.0 for temperatures ≥ 1400 K, i.e., between reaction temperatures of 1200 and 1400 K, more C is deposited at P_{tot} = 0.1 atm than at P_{tot} = 1.0 atm.

(b) For higher CH_4/Al_2O_3 molar ratios (>3.0), deposition efficiency ratios decrease with increasing reaction temperatures, falling below a ratio of 1.0 at temperatures ≥1400 K but increases back up to 1.0 at temperatures ≥1800 K (for intermediate CH_4/Al_2O_3 molar ratios (between 3.00–8.99)) or at temperatures ≥1700 K (for high CH_4/Al_2O_3 ratios (≥8.99)).

(c) Decreasing the P_{tot} to 0.1 atm does not alter the maximum N conversion efficiency from that at P_{tot} = 1.0 atm at temperatures ≥ 1800 K for all CH_4/Al_2O_3 molar ratios (see Figures 15A and 16A). The maximum N conversion efficiency ratio still remains at 1.2 for a maximum Al conversion efficiency of 1.0. However, the C deposition efficiency ratio is 0 (i.e., no C is deposited) for temperatures ≥ 1800 K for CH_4/Al_2O_3 molar ratios ≤ 2.7. This means that low pressures favor the conversion of Al_2O_3 to AlN and retards C deposition for CH_4/Al_2O_3 molar ratios ≤ 2.7.

(d) Decreasing the P_{tot} to 0.1 atm decreases the reaction temperature at which Al and N conversion efficiency ratios are > 1.0, while at the same time C deposition is retarded. The reaction temperature can be decreased from 1800 to 1600 K. The CH_4/Al_2O_3 molar ratio at which lower reaction temperature may be used is 3.00 at both pressures considered. However, though the conversion efficiency ratios are increased, the absolute value for the Al and N conversion efficiencies decrease rapidly as the reaction temperature decreases and are low at temperatures below 1800 K (see Figures 14A,B).

(c) Similar thermodynamic calculations for various NH_3/Al_2O_3 molar ratios show that the effects observed at P_{tot} = 0.1 atm are independent of the NH_3/Al_2O_3 molar ratio, i.e., changing the NH_3/Al_2O_3 ratio did not alter the trends observed as described above.

Introducing excess hydrogen into the system results in C deposition efficiency ratios <1.0 for all CH_4/Al_2O_3 molar ratios considered within the temperature range 1200–2000 K (Figure 17B). There is an increase in C deposition efficiency ratio with increasing temperature from 1200 K up to a maximum at 1400 K, followed by a decrease in C deposition for reaction temperatures > 1400 K. A minimum value is achieved at 1700 K and for CH_4/Al_2O_3 molar ratios > 3.0; the decrease in C deposition is followed by another increase in C deposition and peak maximum at 1800 K. This is followed by another decrease in C deposition at higher temperatures. Addition of hydrogen into the system decreases the reaction temperature to 1700 K (from 1800 K) for an Al conversion efficiency ratio of > 1.0 and a C deposition efficiency of 0. Thus pure AlN may be formed at lower temperatures with the introduction of excess hydrogen into the system.

Figure 17C shows a plot for the C deposition efficiency ratio for a total system pressure of 0.1 atm in the presence of excess hydrogen with respect to reaction temperature for several CH_4/Al_2O_3 molar ratios. Again, the ratio is less than 1.0 for the temperature range 1350–1800 K. The shape of the plots resembles those of Figure 17A for the temperature range 1200–1800 K, while for temperatures higher than 1800 K the trends resemble those of Figure 17B. Since, for low temperatures (1300–1700 K), Al and N conversion efficiency ratios are higher than either low system pressure or introduction of excess hydrogen alone, it would seem advantageous to carry out the conversion at low pressure in the presence of excess hydrogen in the system. However, the absolute Al and N conversion ef-

ficiencies drop rapidly below temperatures of 1800 K. Thus low AlN yields are obtained at low temperatures even though higher conversion efficiency ratios may be obtained at low pressures and in the presence of excess hydrogen.

Conclusions

Computerized thermodynamic analysis of the Al-N-C-H system indicates that pure AlN can be prepared by thermal nitridation of Al_2O_3 using ammonia and methane. Complete conversion of Al_2O_3 to AlN occurs at 1800 K. The reagent concentration ranges within which pure AlN is formed increase with increasing reaction temperature as well as at low pressure in the presence of excess hydrogen. Low pressure together with an excess of hydrogen decreases the reaction temperature at which pure AlN is formed. Low pressure together with the introduction of excess hydrogen into the reaction system increases Al and N conversion efficiency and retards C deposition.

Acknowledgment. We thank Dr. Woo Lee of United Technologies Research Center for helpful discussions. This research has been supported by the State of Connecticut, Department of Higher Education, High Technology Grant Number 42.

Registry No. Al_2O_3, 1344-28-1; NH_3, 7664-41-7; CH_4, 74-82-8; AlN, 24304-00-5.

Ionic Conductivities in Solid Solutions of $K_{5+x}Sb_{5-x}Ti_xP_2O_{20}$ and $K_{5-x}Sb_{5-x}M_xP_2O_{20}$ (M = Mo^{VI}, W^{VI})

B. Wang and M. Greenblatt*

Department of Chemistry, Rutgers—The State University of New Jersey, Piscataway, New Jersey 08855-0939

Received December 11, 1991. Revised Manuscript Received February 10, 1992

Solid solutions of $K_{5+x}Sb_{5-x}Ti_xP_2O_{20}$ ($0 \le x \le 0.2$) and $K_{5-x}Sb_{5-x}M_xP_2O_{20}$ (M = Mo^{VI} and W^{VI}, $0 \le x \le 0.15$) were prepared by solid-state reaction. Ionic conductivity was investigated from 200 to 500 °C by ac complex impedance measurement. The ionic conductivity of the Ti-substituted phase increases with increasing x to the limit of substitution ($x = 0.2$). This increase of conductivity is attributed to a larger bottleneck and an increase in the K^+ concentration due to the Ti substitution. In the Mo/W-substituted phases, the conductivity increases with increasing x to the limit of substitution ($x = 0.15$) due to an increasing K^+ vacancy concentration.

Introduction

Recently, a series of potassium phosphatoantimonates have been reported by Piffard et al.[1-5] The basic building units of these compounds are SbO_6 octahedra and PO_4 tetrahedra with one-, two-, and three-dimensional structures (1D, 2D, and 3D). Some of the potassium phosphatoantimonates also have good ion-exchange properties.[6-8]

Recently, the ionic conductivities of potassium phosphatoantimonates have been studied in our laboratory.[9,10] Of all the potassium phosphatoantimonates studied, $K_5Sb_5P_2O_{20}$ has been found to exhibit the highest ionic conductivity.[9] $K_5Sb_5P_2O_{20}$ has a framework structure in which SbO_6 octahedra share both corners and edges and are also linked to PO_4 tetrahedra via corners. The high ionic conductivity of $K_5Sb_5P_2O_{20}$ compared to the other potassium phosphatoantimonate compounds with different structures is attributed to the skeleton structure (Figure 1) with 3D interconnected, large and mostly vacant tunnels that facilitate the motion of K^+ ions. However, the small bottleneck in this structure[9] limits the fast motion of K^+ ions. It was shown that the conductivity of this phase can be improved by ion exchange of K^+ with smaller cations such as Li^+ and Na^+ or partial substitution of Nb^V or Ta^V for Sb^V to enlarge the bottleneck for K^+ ion motion.[10]

In this work we investigated the effects of aliovalent substitution of antimony on the ionic conductivity of $K_5Sb_5P_2O_{20}$ by replacing some of the Sb^V with Ti^{IV}, Mo^{VI}, and W^{VI} ions. Our objective here was 3-fold:

Table I. Effective Ionic Radii and Electronegatives of Relevant Ions

ion[a]	r[11], Å	χ[12]
Sb^V	0.74	1.763
Ti^{IV}	0.75	1.577
Mo^{VI}	0.73	2.025
W^{VI}	0.74	2.132

[a] CN: 6.

(1) To study the effect of changes in the K^+ ion concentration and K^+ ion vacancy concentration. When tetravalent titanium ions or hexavalent molybdenum or tungsten ions are substituted for pentavalent antimony ions, one expects K^+ ion concentration and K^+ ion vacancy concentration to increase respectively, with concomitant

* To whom correspondence should be addressed.

(1) Lachgar, A.; Deniard-Courant, S.; Piffard, Y. *J. Solid State Chem.* **1986**, *63*, 409.
(2) Piffard, Y.; Oyetola, S.; Courant, S.; Lachgar, A. *J. Solid State Chem.* **1985**, *60*, 209.
(3) Piffard, Y.; Lachgar, A.; Tournoux, M. *J. Solid State Chem.* **1985**, *58*, 253.
(4) Piffard, Y.; Lachgar, A.; Tournoux, M. *Mater. Res.* Bull. **1986**, *21*, 1231.
(5) Piffard, Y.; Lachgar, A.; Tournoux, M. *Mater. Res. Bull.* **1985**, *20*, 715.
(6) Piffard, Y.; Verbaere, A.; Oyetola, S.; Deniard-Courant, S.; Tournoux, M. *Eur. J. Solid State Inorg. Chem.* **1989**, *26*, 113.
(7) Piffard, Y.; Verbaere, A.; Lachgar, A.; Deniard-Courant, S.; Tournoux, M. *Rev. Chim. Miner.* **1986**, *23*, 766.
(8) Tournoux, M.; Piffard, Y. French Patent 85-10839.
(9) Wang, E.; Greenblatt, M. *Chem. Mater.* **1991**, *3*, 542.
(10) Wang, E.; Greenblatt, M. *Chem. Mater.* **1991**, *3*, 703.
(11) Shannon, R. D. *Acta Crystallogr.* **1976**, *A32*, 751.
(12) Zhang, Y. *Inorg. Chem.* **1982**, *21*, 3886.

0897-4756/92/2804-0657$03.00/0